BIOCHEMISTRY
including biophysical chemistry & molecular biology

Article

pubs.acs.org/biochemistry

Open Access on 05/23/2015

Probing the Non-Native H Helix Translocation in Apomyoglobin Folding Intermediates

Phillip C. Aoto, Chiaki Nishimura, H. Jane Dyson, and Peter E. Wright*

Department of Molecular Biology and Skaggs Institute of Chemical Biology, The Scripps Research Institute, 10550 North Torrey Pines Road, La Jolla, California 92037, United States

Supporting Information

ABSTRACT: Apomyoglobin folds via sequential helical intermediates that are formed by rapid collapse of the A, B, G, and H helix regions. An equilibrium molten globule with a similar structure is formed near pH 4. Previous studies suggested that the folding intermediates are kinetically trapped states in which folding is impeded by non-native packing of the G and H helices. Fluorescence spectra of mutant proteins in which cysteine residues were introduced at several positions in the G and H helices show differential quenching of W14 fluorescence, providing direct evidence of translocation of the H helix relative to helices A and G in both the kinetic and equilibrium intermediates. Förster resonance energy transfer measurements show that a 5-({2-[(acetyl)amino]ethyl}amino)naphthalene-1-sulfonic acid acceptor coupled to K140C (helix H) is closer to Trp14 (helix A) in the equilibrium molten globule than in the native state, by a distance that is consistent with sliding of the H helix in an N-terminal direction by approximately one helical turn. Formation of an S108C−L135C disulfide prevents H helix translocation in the equilibrium molten globule by locking the G and H helices into their native register. By enforcing nativelike packing of the A, G, and H helices, the disulfide resolves local energetic frustration and facilitates transient docking of the E helix region onto the hydrophobic core but has only a small effect on the refolding rate. The apomyoglobin folding landscape is highly rugged, with several energetic bottlenecks that frustrate folding; relief of any one of the major identified bottlenecks is insufficient to speed progression to the transition state.

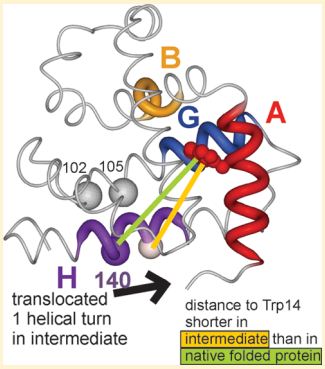

Obtaining information about specific interatomic distances during the process of protein folding is challenging. Although nuclear Overhauser effects can potentially provide a great deal of distance information, the nuclear magnetic resonance (NMR) technique is inherently slow and cannot directly probe distance changes on the microsecond to millisecond time scales relevant to most kinetic protein folding processes. Indirect NMR methods using rapid mixing quench-flow hydrogen−deuterium exchange[1,2] or chemically induced dynamic nuclear polarization,[3] and real-time NMR experiments have been successfully used to probe slow protein folding pathways.[4−6] Fluorescence spectroscopy is inherently a faster technique and has been extensively used for studies of folding processes, utilizing stopped-flow methods, but has a disadvantage in that it gives information about only a limited set of distances near tryptophan side chains. The information available from fluorescence experiments can be amplified by the introduction of other fluorogenic probes into the molecule, which can then be used in concert with natural or engineered tryptophan residues to provide distance information through Förster resonance energy transfer (FRET).

We have used a variety of biophysical techniques, including quench-flow hydrogen−deuterium exchange detected by NMR and mass spectrometry, stopped-flow kinetics detected by CD and fluorescence, small-angle X-ray scattering, and equilibrium NMR, fluorescence, and CD measurements, to study the equilibrium and kinetic folding intermediates of wild-type sperm whale apomyoglobin and various designed mutants.[7−22] Apomyoglobin folds via two sequential on-pathway intermediates (I_a or I_1 and I_b or I_2) that are formed within a few milliseconds of initiation of refolding, followed by a slower folding phase to the native state.[22−25] The structure of the burst phase kinetic intermediate I_b formed after 5 ms has been found to be very similar, but not identical, to that of an equilibrium intermediate formed at pH 4.[7,16,21] Important insights into the structure of the apomyoglobin folding intermediate were provided by studies of a series of mutants[16,19] that suggested that the helices that form the core of the kinetic intermediate dock in a nativelike topology. These studies also revealed non-native interactions between helices G and H that arise from translocation of the H helix by approximately one helical turn toward its N-terminus.[19] Resolution of these non-native contacts would therefore be required before the protein molecule could proceed to form the native folded structure. We hypothesize that both the kinetic and equilibrium intermediates contain the A and G helices docked securely in a nativelike topology, with the H helix also docked to this core, but translocated by one helical turn relative to the G helix. To test this hypothesis, we have designed mutants of apomyoglobin, replacing selected residues in the G and H helices with cysteine, which causes distance-dependent quenching of the

Received: April 21, 2014
Revised: May 22, 2014
Published: May 23, 2014

fluorescence of the tryptophan at position 14 in the A helix of apomyoglobin, giving insights into the distances among the A, G, and H helices under various solution conditions. Following attachment of the fluorescence acceptor AEDANS to selected single-cysteine mutants, we have used FRET from the native tryptophan at position 14 to probe for the presence of non-native structure in the equilibrium apomyoglobin intermediate at intermediate pH values. A double-cysteine mutant containing a disulfide bond between the G and H helices was also examined to determine the effects on the folding pathway, and particularly on the rate-determining step (correct docking of the E helix), of constraining the G and H helices into a nativelike packing topology in the earliest stages of folding. The results confirm the presence of a translocation in the H helix in the apomyoglobin kinetic folding intermediate and provide new insights into the role of energetic frustration in facilitating progression to the native state by preventing excessive stabilization of non-native contacts within the compact folding intermediates.

MATERIALS AND METHODS

Preparation of Protein. Sperm whale apoMb was overexpressed in *Escherichia coli* BL21-DE3 cells with a pET17b vector containing the Mb gene as previously described.[26] Site-directed mutagenesis to obtain the mutant genes (W7F for all single-cysteine mutants, followed by replacement of K77, K102, Y103, E105, F106, I111, M131, L135, F138, R139, K140, Y146, or K147 with cysteine, or S108C/L135C for the double-cysteine mutant) was conducted using the QuikChange Site-Directed Mutagenesis Kit (Stratagene). Isotopically labeled and unlabeled mutant proteins were produced in M9 minimal medium and purified as previously described.[26] Minimal medium is preferred even for unlabeled samples, because the protein yield is sufficiently high (~70 mg/L) and the purification procedure is easier than for protein derived from growth in rich medium such as LB.

Incorporation of the Fluorescence Acceptor. Chemical modification at the single cysteine in the Cys-incorporated mutants was performed by reaction with the thiol-specific probe 5-({2-[(iodoacetyl)amino]ethyl}amino)naphthalene-1-sulfonic acid (IAEDANS) (Molecular Probes) in 100 mM Tris-HCl buffer at pH 8.5 after reducing any possible intermolecular disulfide bonds of the cysteine-incorporated mutants with 10 mM DTT. The reaction was performed at 4 °C for 16 h, yielding a protein with the 5-({2-[(acetyl)amino]-ethyl}amino)naphthalene-1-sulfonic acid group (AEDANS) covalently attached to the cysteine thiol. The AEDANS-labeled protein was purified by using a Sephadex G15 column (Pharmacia) to remove the free IAEDANS. The protein solution was concentrated and buffer-exchanged to water by using a Centriprep 10 cartridge (Amicon).

The extinction coefficient used to obtain the protein concentration of the W7F single-cysteine mutant (10400 M^{-1} cm^{-1} at 280 nm) was calculated from the extinction coefficient of the wild-type (W7 and W14) protein (15900 M^{-1} cm^{-1} at 280 nm and pH 6.1).[27] The efficiency of labeling was determined spectrophotometrically by comparing the absorbance at 336 nm (extinction coefficient of AEDANS[28] of 6160 M^{-1} cm^{-1}) with the absorbance at 280 nm (extinction coefficients of 10400 M^{-1} cm^{-1} for protein and 1310 M^{-1} cm^{-1} for AEDANS). A 1:1 AEDANS:protein stoichiometry was confirmed for all proteins, using the 336 nm/280 nm absorbance ratio.

Oxidation of the Two-Cysteine Mutant. An intramolecular disulfide bond was formed between S108C and L135C by incubating 20 μM refolded two-cysteine mutant in 50 mM Tris-HCl (pH 7.7), 1 mM EDTA, 0.01 mM DTT, and 5 mM oxidized glutathione at 4 °C overnight. The progress of oxidation was monitored by analytical high-performance liquid chromatography (HPLC). The oxidized (disulfide) two-cysteine mutant was diluted into a 0.1% TFA/water mixture and purified from reduced (dithiol) and intermolecular disulfide forms by reverse phase HPLC with a linear gradient of 100% acetonitrile in 0.1% TFA. Lyophilized protein was checked for the absence of reduced and oligomeric forms by analytical HPLC and matrix-assisted laser desorption ionization time-of-flight mass spectrometry. The fully reduced form of the two-cysteine mutant was purified in the presence of 5 mM DTT.

Circular Dichroism (CD) Spectroscopy. CD spectra were recorded on an Aviv 62DS spectrometer at 25 °C. The ellipticity of the proteins (10 μM for all single- and double-cysteine mutants) in 10 mM sodium acetate buffer was monitored at 222 nm as a function of pH from pH 6 to 2 or of added urea up to 8.5 M.

NMR Spectroscopy. Multidimensional NMR experiments were performed on Bruker Avance 500, DRX600, and DRX800 spectrometers equipped with cryogenic probes, and Avance 750 and Avance 900 spectrometers with room-temperature probes. All NMR data were collected with ^{1}H- and ^{15}N-labeled protein in 10 mM sodium acetate buffer, 0.01% (v/v) NaN_3, and 10% (v/v) D_2O at pH 6.1 and 30 °C or at pH 4.1 and 46 °C with 10% (v/v) ethanol. Spectra of the reduced form of the two-cysteine mutant were recorded in the presence of 1 mM DTT. Doubly labeled (^{13}C and ^{15}N) protein samples were used for backbone resonance assignment.

$^{1}H-^{15}N$ HSQC spectra of oxidized and reduced forms of the two-cysteine mutant and wild-type apomyoglobin were recorded at pH 6.1 and 4.1 using the States–TPPI method[29] for data acquisition in the indirect dimension. Backbone resonance assignments for the two-cysteine mutant were made using constant-time three-dimensional (3D) HNCA,[30] 3D HNCOCA,[30] and 3D ^{15}N NOESY-HSQC (nuclear Overhauser enhancement spectroscopy) spectra[31] at pH 6.1 and 4.1. Steady state $\{^{1}H\}-^{15}N$ heteronuclear NOE[32] data were collected in triplicate at pH 4.1 for the oxidized two-cysteine mutant and for wild-type apomyoglobin with a NOE buildup time of 3 s and a recycle delay of 3.5 s.

NMR data were processed with NMRPipe[33] and analyzed with NMRView.[34] Sequence-specific secondary chemical shifts were determined as previously described.[35]

Fluorescence Spectroscopy. All fluorescence spectra were recorded on a Fluorolog-3 fluorescence spectrometer (Jobin Yvon-Horiba) at 25 °C. Fluorescence emission spectra of the W7F, W7F/I111C, W7F/M131C, and W7F/L135C mutants were recorded at a concentration of 2 μM in 10 mM sodium acetate buffer containing 0.5 mM DTT. Emission spectra of the S108C/L135C mutant protein in the oxidized form were obtained at a concentration of 5 μM in 10 mM sodium acetate buffer, with excitation at 288 nm. The excitation and emission bandwidths were set at 2 nm, and the emission spectra were scanned from 300 to 400 nm for each sample. Acid unfolding curves were measured by monitoring the intensity at the emission maximum as a function of pH. Individual samples were prepared for each pH data point.

dx.doi.org/10.1021/bi500478m | *Biochemistry* 2014, 53, 3767–3780

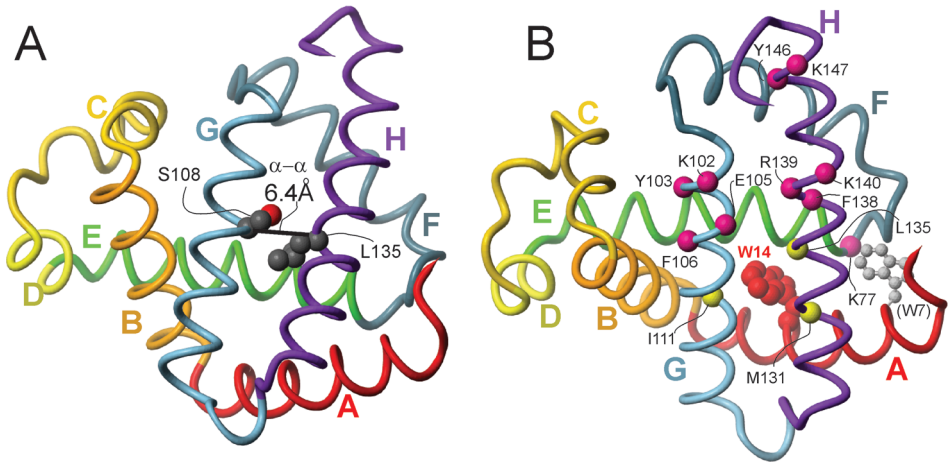

Figure 1. Backbone chain trace of holomyoglobin.[51] (A) Location of the residues, S108 and L135 (spheres), mutated to form the disulfide mutant. The S108–L135 Cα–Cα distance is shown. (B) Sites of the mutations used for fluorescence quenching and FRET studies and location of the two tryptophan residues. W7 (gray) was mutated to Phe for all of the FRET and fluorescence quenching experiments. The Cα positions of residues mutated in the FRET experiments are colored pink. The Cα positions of residues mutated in the cysteine fluorescence quenching experiments are colored yellow.

Stopped-Flow Kinetics. The kinetics of refolding of the W7F, W7F/M131C, and W7F/L135C mutants and the oxidized S108C/L135C mutant were measured at 8 °C using a DX-17MV Applied Photophysics stopped-flow instrument. The excitation wavelength was 288 nm with an excitation slit width of 1 nm. The fluorescence signal was recorded with a 320 nm cutoff filter. Refolding of the W7F, W7F/M131C, and W7F/L135C mutants was monitored by measuring the change in fluorescence emission following a pH jump from pH 2.2 to 6.0 by a 1:5 dilution with 30 mM sodium acetate buffer containing 0.5 mM DTT. The final protein concentration was 2 μM after mixing. The refolding kinetics of the disulfide-bridged mutant were measured using both pH jump and urea dilution methods. S108C/L135C apomyoglobin (30 μM), in both the oxidized and reduced forms, was unfolded in a solution containing 8 M urea in refolding buffer [10 mM sodium acetate (pH 6.1)] and refolded by 6-fold dilution in the stopped-flow apparatus to a final urea concentration of 1.3 M. Refolding of the oxidized double-cysteine mutant by a pH jump from pH 2.5 to 6.0 was performed with a 1:5 dilution of 30 μM apomyoglobin into 30 mM sodium acetate buffer.

Refolding kinetics of the W7F/M131C and W7F/L135C mutants were also measured at 8 °C by stopped-flow CD. The ellipticity at 225 nm was measured with a slit width of 2 nm. Refolding was initiated by a pH jump from pH 2.2 to 6.0 by a 1:5 dilution with 30 mM sodium acetate buffer. The final concentration of protein was 10 μM after mixing. The dead time of the instrument for CD measurements is ~10 ms.

Förster Resonance Energy Transfer (FRET). Emission spectra derived from the fluorescence of tryptophan at position 14 were recorded. The emission spectra of the W7F, single-cysteine mutant proteins and their corresponding AEDANS adducts (2 μM) in 10 mM sodium acetate buffer were recorded from 300 to 500 nm. The excitation wavelength was set at 280 nm with the bandwidth of both excitation and emission set at 2 nm. The maximal intensities of the Trp fluorescence or AEDANS emission were plotted as a function of pH. In both studies, separate samples were prepared for each data point.

Analysis of FRET Data. Comparison of the fluorescence intensity between each AEDANS-labeled protein and the corresponding unlabeled cysteine mutant (transfer efficiency $E = 1 - F/F_0$, where F_0 is the emission intensity of the donor alone and F is the measured emission intensity of the donor tryptophan in the presence of the acceptor) allows estimation of the donor–acceptor distance. Energy transfer by the dipolar interaction is described by the Förster equation:[36]

$$E = R_0^6/(r^6 + R_0^6)$$

where E is the energy transfer efficiency, R_0 is the Förster distance, at which the energy transfer rate is equal to the decay rate, i.e., 50% fluorescence energy transfer efficiency, and r is the donor–acceptor distance.

The magnitude of R_0 is dependent on the spectral properties of the donor and acceptor groups:[37]

$$R_0 = [8.785 \times 10^{-5} \times \kappa^2 n^{-4} \phi_D \times J(\lambda)]^{1/6} \text{ Å}$$

where κ^2 is the dipole orientation factor (range of 0–4; $\kappa^2 = {}^2/_3$ for randomly oriented donors and acceptors), ϕ_D is the fluorescence quantum yield of the donor in the absence of the acceptor, n is the refractive index, and $J(\lambda)$ is the spectral overlap integral

$$J(\lambda) = \int \varepsilon_A(\lambda) \times F_D(\lambda) \times \lambda^4 \, d\lambda \text{ cm}^3 \text{ M}^{-1}$$

where ε_A is the extinction coefficient of the acceptor and F_D is the fluorescence emission intensity of the donor as a fraction of the total integrated intensity.

In the case of the AEDANS/Trp pair, the value of R_0 is assumed to be 22 Å.[37] On the basis of this value, the value of r (distance between W14 and incorporated AEDANS) was estimated for the mutant proteins under different conditions.

RESULTS

Design of Mutant Proteins. The locations of the various mutation sites are mapped onto the three-dimensional structure of sperm whale holomyoglobin in Figure 1. The structure of apomyoglobin is very similar to that of the holoprotein except that residues in helix F, the E–F and F–G loops, and the C-terminal region of helix H are dynamically disordered in the apo form.[38,39] The tryptophan side chain has an absorbance maximum at 280 nm and a fluorescence emission maximum at

dx.doi.org/10.1021/bi500478m | Biochemistry 2014, 53, 3767–3780

~336 nm; tryptophan can be used as a fluorescence donor with excitation at 280 nm. The two tryptophan residues in sperm whale myoglobin, W7 and W14, are both located in the A helix. Of the two, W14 is preferred for use as a fluorescence donor for probing the folding intermediates because of its location in the center of the A helix (Figure 1). To simplify the data analysis, W7 was substituted with phenylalanine in all of the mutant proteins prepared for study by fluorescence or FRET, so that the fluorescence quenching or FRET signals would arise from the proximity of W14 to the cysteine quenching group or the AEDANS fluorescence acceptor coupled at various sites in the E, G, and H helices. Because there is no native cysteine in sperm whale myoglobin, it was a relatively simple matter to change the residues of interest to cysteine.

The design of suitable double-cysteine mutants for the introduction of a disulfide between the G and H helices was complicated by the need to avoid structural strain as a consequence of formation of the disulfide. A number of double-cysteine mutations were introduced, including some designed to lock the G and H helices into the putative "translocated" conformation in the intermediate (Table S1 of the Supporting Information). For all mutants in which the disulfide bond was not carefully designed to mimic the native folded structure, i.e., with nativelike G−H helix packing, we had difficulties either in the expression of the protein in *E. coli* or in the formation of the disulfide bond. For some mutants, formation of the disulfide bond caused irreversible aggregation and precipitation of the protein. However, the S108C/L135C double mutant proved to be well behaved in the reduced and oxidized states in solution, likely because of the similarity of the Cα−Cα distance (6.4 Å) between S108 and L135 in the wild-type protein (Figure 1B) and the Cα−Cα distance in a disulfide bond (4.4−6.8 Å[40,41]).

Spectroscopic Characterization of the One- and Two-Cys Mutants. Site-directed mutagenesis of apomyoglobin generally results in the formation of proteins that strongly resemble the wild-type protein in structure and are generally well-behaved in solution.[10,13,14,16,19,20] The integrity of the folded state of each mutant was checked carefully, using CD and in some cases NMR spectroscopy. The spectra of the mutant proteins are all very similar to that of the wild-type protein, indicating that they adopt similar folded states (Figures S1 and S2 of the Supporting Information).

The oxidized S108C/L135C mutant was subjected to detailed NMR analysis to confirm that formation of the disulfide did not perturb the structure. HSQC spectra at pH 6.1 are well dispersed and confirm that the mutant protein is fully folded (Figure S2A of the Supporting Information). Backbone amide assignments and ^{13}Cα resonances were assigned for 117 residues in the oxidized protein for the pH 6.1 native state. As for WT apomyoglobin,[38] the backbone resonances of residues 82−106, in the F helix, F−G loop, and N-terminal region of the G helix, and residues 139−141 and 146−148 in the C-terminal region of the H helix are broadened beyond detection by conformational fluctuations.[38] Analysis of the ^{15}N, ^{1}HN, and ^{13}Cα chemical shifts using Talos+[42] indicates that the helical secondary structure of the oxidized S108C/L135C double mutant is identical to that of WT. The HSQC spectra of the WT and oxidized and reduced mutants at pH 4.1 are poorly dispersed with differentially broadened cross peaks, as expected for the disordered molten globular intermediate[12] (Figure S2B of the Supporting Information). Assignments could be made for 126 of a possible 148 amide cross peaks, excluding the N-terminus and Pro residues, and ^{13}Cα resonances could be assigned for 135 and 140 residues for oxidized S108C/L135C and WT protein, respectively. The amide chemical shift differences between the disulfide-bridged mutant and the wild-type protein are shown in Figure 2A at pH 6.1 and in

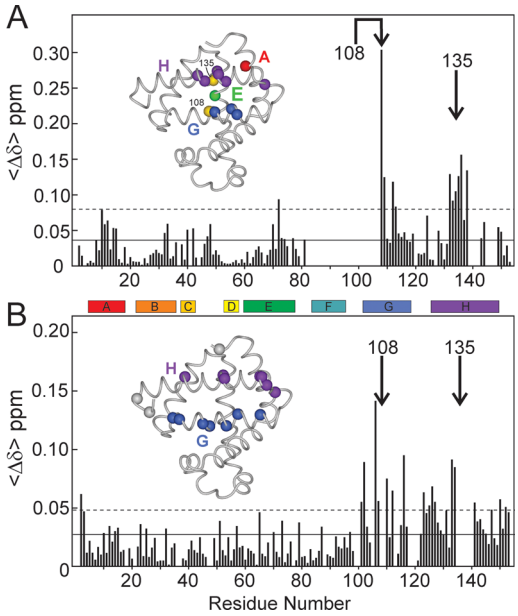

Figure 2. Comparison of chemical shifts of wild-type apomyoglobin and the oxidized S108C/L135C mutant. (A) Difference in the weighted average backbone HN and ^{15}N chemical shifts $\{\langle\Delta\delta\rangle = {}^{1}/_{2}[(\Delta\delta_{HN})^2 + (\Delta\delta_{N}/5)^2]^{1/2}\}$ between the wild type and oxidized two-cysteine mutant at pH 6.1. The location of the mutations is indicated by arrows. Horizontal lines represent the mean and (mean + 1 standard deviation) of the $\langle\Delta\delta\rangle$ values. The inset shows major chemical shift changes at pH 6.1 mapped onto the structure of Mb.[51] Positions of helices A−H are indicated by colored bars. Spheres colored according to the helix location represent the backbone N atoms of residues where the composite $\Delta\delta$ > (mean + 1 standard deviation). Yellow spheres show the positions of the mutated residues. (B) Difference in the weighted average backbone HN and ^{15}N chemical shifts ($\langle\Delta\delta\rangle$) between the wild type and oxidized two-cysteine mutant at pH 4.1. The location of the mutations is indicated by arrows. Horizontal lines represent the mean and (mean + 1 standard deviation) of the $\langle\Delta\delta\rangle$ values. The inset shows major chemical shift changes at pH 4.1 mapped onto the structure of Mb.[51] Colored spheres represent the backbone N atoms of residues where the composite $\Delta\delta$ > (mean + 1 standard deviation).

Figure 2B at pH 4.1. The secondary ^{13}Cα chemical shifts, i.e., the deviation of observed chemical shifts from sequence-corrected random coil values, for the oxidized mutant and wild-type proteins are shown in Figure 3A. The backbone amide and ^{13}Cα chemical shifts of the WT and mutant proteins are very similar, with differences mostly localized to the sites of mutation and the G−H helix region. The NMR data show that the overall structure of the molten globule state formed by the disulfide-bridged mutant is very similar to that of WT. However, small changes in ^{13}Cα chemical shifts (Figure 3B) and increases in the heteronuclear NOE (Figure 3C) indicate small localized differences in secondary structure and dynamics. Most notably, the ^{13}Cα shift changes are consistent with an increase in helical content for H116 and S117, near the C-terminus of helix G, and for A125, D126, and Q128 in the first turn of the H helix. This stabilization of helical structure is accompanied by an increase in the heteronuclear NOE,

dx.doi.org/10.1021/bi500478m | *Biochemistry* 2014, 53, 3767−3780

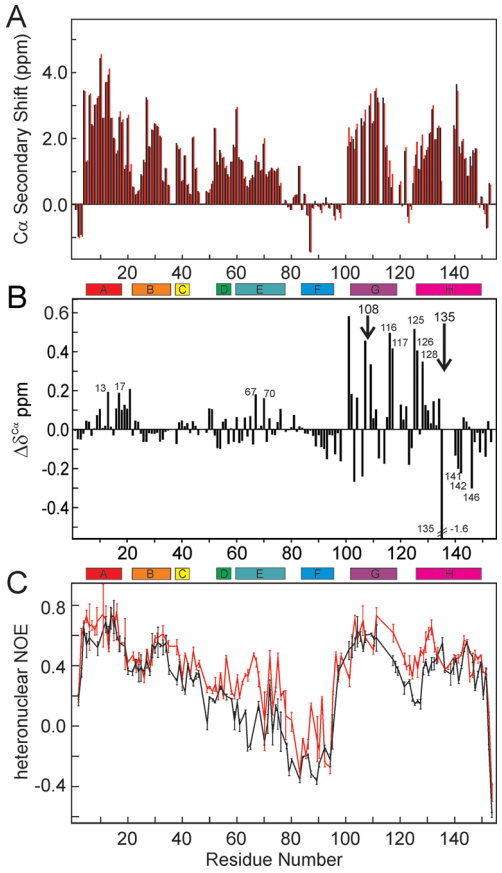

Figure 3. (A) Secondary $^{13}C\alpha$ chemical shifts (observed chemical shift minus the sequence-corrected random coil shift) for the wild type (black) and oxidized two-cysteine mutant (red) at pH 4.1. (B) Difference $[\Delta\delta^{C\alpha} = \delta^{C\alpha}(\text{mutant}) - \delta^{C\alpha}(\text{WT})]$ between the $^{13}C\alpha$ chemical shifts in panel A. (C) Heteronuclear $\{^1H\}-^{15}N$ NOE at pH 4.1 for the wild type (black) and oxidized two-cysteine mutant (red).

consistent with decreased backbone flexibility due to enhanced packing onto the molten globule core. At the same time, there appears to be a slight decrease in helicity at the C-terminal end of the H helix, as indicated by a decrease in the secondary chemical shift of residues D141, I142, and Y146. The observed structural and dynamic changes suggest that the constraints imposed by the S108C/L135C disulfide bridge prevent translocation of the H helix, allowing better packing of the N-terminal region of helix H and an accompanying increase in helicity, while destabilizing the C-terminal end of helix H. It is of interest that small $^{13}C\alpha$ chemical shift perturbations are observed for V13 and V17, residues in the A helix region that would contact the C-terminal end of helix G and the F−G turn in the native myoglobin topology. Small $^{13}C\alpha$ chemical shift changes also occur in the middle of the E helix (T67 and T70), a region that shows increased heteronuclear NOEs that suggest enhanced packing into the molten globule core.

Equilibrium Unfolding Experiments. The unfolding behavior of apomyoglobin upon addition of denaturant or a decrease in pH is well-documented.[9,43,44] By performing such denaturation experiments on the mutant proteins, we obtain valuable insights into local and global effects of the mutations and their influence on equilibrium unfolding processes. Apomyoglobin undergoes unfolding transitions as the pH is lowered from 6 to 2, or upon addition of high concentrations of urea or guanidine hydrochloride.[7] These unfolding transitions can be monitored by CD, following the loss of helical structure, or by tryptophan fluorescence, which is differentially quenched in the folded (pH 6), intermediate (pH 4), and acid-unfolded (pH 2) states. The signature of the molten globule equilibrium intermediate formed at pH 4 is a maximum in fluorescence intensity,[45] where the tryptophan fluorescence (primarily W14) is quenched neither by the proximity to the sulfur of M131 (as in the native state at pH 6) nor by contact with the solvent in the unfolded states formed at more acidic pH.

The CD and fluorescence spectra of the S108C/L135C double mutant and wild-type proteins as a function of pH or of added denaturant are shown in Figure 4. The oxidized S108C/L135C mutant forms a partly folded intermediate near pH 4,

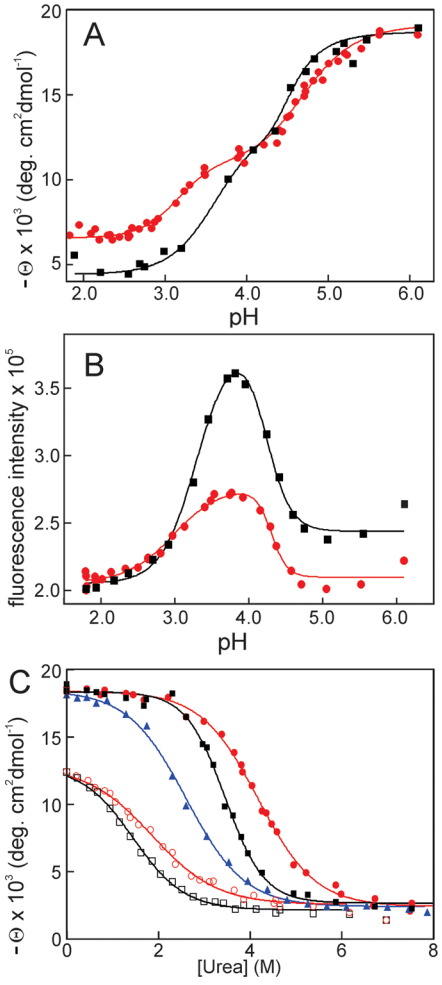

Figure 4. Variation in CD and fluorescence signals with pH and urea. (A) pH dependence of the mean residue ellipticity at 222 nm for wild-type apomyoglobin (black) and the oxidized two-cysteine mutant (red). Solid curves are fit to the data using the method of least squares to a three-state unfolding model. (B) pH dependence of the fluorescence signal at the emission maximum upon excitation at 288 nm for wild-type apomyoglobin (black) and the oxidized two-cysteine mutant (red). Solid curves are fit to the data using the method of damped least squares to a three-state unfolding model. (C) Urea dependence of the mean residue ellipticity at 222 nm for wild-type apomyoglobin (black) at pH 6.1 (filled squares) and pH 4.1 (empty squares), the oxidized two-cysteine mutant (red) at pH 6.1 (filled circles) and pH 4.1 (empty circles), and the reduced two-cysteine mutant (blue) at pH 6.1 (filled triangles). Data were fit by the method of least squares to a two-state unfolding model.

dx.doi.org/10.1021/bi500478m | *Biochemistry* 2014, 53, 3767−3780

with a helical content comparable to that of the molten globule intermediate formed by the WT protein (Figure 4A). At more acidic pH, however, the mutant exhibits greater ellipticity than the WT. Urea denaturation curves (Figure 4C) show that the native state (pH 6.1) of the S108C/L135C mutant is cooperatively folded in both the oxidized and reduced states. Introduction of the two cysteines slightly destabilizes the apomyoglobin toward urea denaturation, but formation of the disulfide increases the stability by 1.7 kcal/mol and shifts the denaturation curve to higher urea concentrations than for the WT. Thermodynamic parameters for urea denaturation of the native state and the pH 4.1 intermediate are summarized in Table 1.

Table 1. Thermodynamic Parameters for the Disulfide-Bonded Mutant

	wild type	108−135 ox	108−135 red
	Urea Titration at pH 6.1		
$\Delta G(H_2O)$ (kcal mol^{-1})	−5.1 ± 0.2	−4.8 ± 0.1	−3.1 ± 0.2
m (kcal mol^{-1})	1.42 ± 0.05	1.16 ± 0.03	1.12 ± 0.06
C_m (M)	3.6	4.1	2.8
	Urea Titration at pH 4.1		
$\Delta G(H_2O)$ (kcal mol^{-1})	−1.4 ± 0.2	−1.3 ± 0.1	–
m (kcal mol^{-1})	1.02 ± 0.08	0.79 ± 0.03	–
C_m (M)	1.4	1.6	–

Probing the Structure of the Equilibrium Intermediate by Fluorescence Quenching. Cysteine is a highly efficient intramolecular quencher of tryptophan fluorescence; quenching occurs at a very short range through direct contact between the Trp and Cys side chains.[46,47] We utilized this property to probe contacts between W14 in the A helix and Cys probes introduced at specific sites in the G helix (I111C) and H helix (M131C and L135C). To simplify the analysis, W7 was substituted with phenylalanine in all of the mutant constructs. Quenching of the fluorescence of the remaining tryptophan residue by the incorporated Cys therefore reflects static or dynamic contacts between the Cys side chain and the W14 indole. W7F is a conservative mutation, found in many myoglobin sequences;[48] this mutation does not perturb the secondary or tertiary structure of apomyoglobin.[49,50]

The pH dependence of the W14 fluorescence emission intensity in the W7F, W7F/I111C, W7F/M131C, and W7F/L135C mutants is shown in Figure 5. The emission maximum for W7F, corresponding to the pH at which the population of the molten globule intermediate is maximal, occurs at higher pH (4.4) than for wild-type apomyoglobin (pH 4.0) (Figure 4B), reflecting destabilization of both the native state and the intermediate by the W7F mutation.[49] The pH-induced unfolding curve for W7F/I111C is very similar to that of W7F except for a slight increase in the level of fluorescence quenching in the pH 4.4 intermediate, suggesting a slight decrease in the distance between these side chains in the intermediate relative to the native state. By contrast, the titration curve of W7F/M131C is significantly different from that of W7F. At pH 6, the intensity is much lower than that of W7F, which we attribute to an increased level of W14 fluorescence quenching because of the proximity of the W14 and C131 side chains in the native structure (the Met131 side chain makes direct contact with the indole ring in the X-ray structure of holomyoglobin). However, the W14 fluorescence intensity for W7F/M131C in the pH ∼4.5 intermediate is the same as that for W7F, indicating no quenching by the Cys at position 131 in the molten globule state. For W7F/L135C, the cysteine at 135 is distant from the indole ring of W14 in the native state (∼7 Å in the X-ray structure of holomyoglobin) and fails to quench the W14 fluorescence at pH 6. However, C135 strongly quenches the tryptophan fluorescence in the intermediate formed at pH ∼4.5 (Figure 5), indicating close, non-native contact between the cysteine and tryptophan side chains in the equilibrium molten globule state. Taken together, the fluorescence quenching data for this set of mutants provide strong support for a structural model in which the H helix is displaced in an N-terminal direction in the equilibrium molten globule, bringing the side chain of residue 135 into non-native contact with W14.

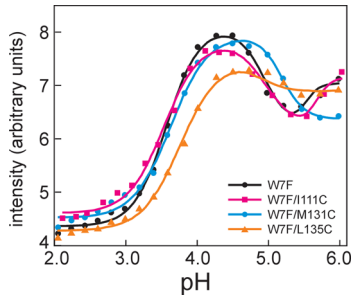

Figure 5. pH dependence of the quenching of the fluorescence of W14 induced by the presence of cysteine at positions 111, 131, and 135. All proteins contained the W7F mutation: W7F (filled black circles, black line), W7F/M131C (filled blue circles, blue line), W7F/L135C (filled orange triangles, orange line), and W7F/I111C (filled magenta squares, magenta line). The maximal intensity of the fluorescence emission was recorded with an excitation wavelength of 288 nm.

Translocation of the H Helix in the Kinetic Intermediate. Kinetic refolding of apomyoglobin, as measured by stopped-flow CD or fluorescence spectroscopy, occurs in two phases, an initial "burst" phase that is complete within the dead time of the apparatus and a slower (approximately milliseconds) phase that can be monitored directly. The refolding kinetics of the W7F, W7F/M131C, and W7F/L135C mutants were monitored using stopped-flow fluorescence and CD measurements. The changes in W14 fluorescence emission during kinetic refolding are shown in Figure 6. The kinetic traces for W7F and W7F/M131C are biphasic, reporting on the rates of the $I_a \rightarrow I_b$ and $I_b \rightarrow N$ folding processes,[23] and were fit to double-exponential decays. For W7F/L135C, the change in fluorescence emission during the slow phase ($I_b \rightarrow N$) is of extremely small amplitude, because there is little change in fluorescence intensity between the molten globule and native

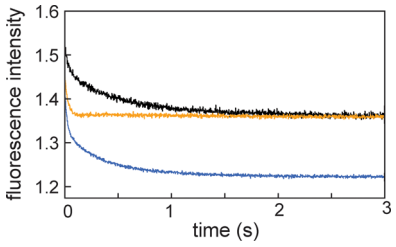

Figure 6. Fluorescence decay after a pH jump from pH 2.2 to 6.0 for W7F (black), W7F/M131C (blue), and W7F/L135C (orange). The stopped-flow traces show total fluorescence with a 320 nm cutoff filter. The excitation wavelength was 288 nm.

dx.doi.org/10.1021/bi500478m | Biochemistry 2014, 53, 3767−3780

state (Figure 5), and the fast phase dominates the stopped-flow trace (Figure 6). The fitted kinetic parameters are summarized in Table 2.

Table 2. Kinetic Parameters for Folding of the Cysteine Mutants

	W7F	W7F/M131C	W7F/L135C
Stopped-Flow Refolding pH Jump (2.2 → 6.0) Two-Exponential Fit (fluorescence)			
k_1 (s^{-1})	30 ± 2	46 ± 1	37 ± 1
k_2 (s^{-1})	1.87 ± 0.03	2.62 ± 0.02	(0.34 ± 0.25)[a]
Stopped-Flow Refolding pH Jump (2.2 → 6.0) Two-Exponential Fit (CD)			
k (s^{-1})		2.5 ± 0.2	2.2 ± 0.1
	wild type	108SH−135SH	108−135 SS
Stopped-Flow Refolding Urea Jump (8 → 1.3 M)			
k (s^{-1})	2.20 ± 0.02	3.05 ± 0.02	5.38 ± 0.02
Stopped-Flow Refolding pH Jump (2.5 → 6.0) Two-Exponential Fit			
k_1 (s^{-1})	22.9 ± 0.7		27.7 ± 0.6
k_2 (s^{-1})	3.43 ± 0.03		4.42 ± 0.03

[a]This rate was derived from the biexponential fit; however, the amplitude of the fluorescence change is close to zero, so it is likely that this does not represent a folding transition.

The overall rate of refolding of the W7F/M131C and W7F/L135C mutants to the fully helical native structure was measured by stopped-flow CD. The $I_a \rightarrow I_b$ transition is not resolved by conventional stopped-flow CD refolding measurements in which folding is initiated by a pH jump to pH 6.0.[7,24] Under these conditions, stopped-flow CD monitors the stabilization of helical structure that occurs during the $I_b \rightarrow N$ transition. The stopped-flow CD traces for W7F/M131C and W7F/L135C were fit to single-exponential curves with rates of 2.5 ± 0.2 and 2.2 ± 0.1 s^{-1}, respectively. The rate for W7F/M131C is in excellent agreement with the k_2 ($I_b \rightarrow N$) obtained from the biphasic fits of the fluorescence refolding curves (Table 2). The stopped-flow CD measurements yield the rate of the $I_b \rightarrow N$ transition for W7F/L135C (2.2 s^{-1}), which could not be resolved by stopped-flow fluorescence.

The stopped-flow experiments also provide new insights into the structure of the apoMb kinetic folding intermediates. The I_a intermediates of the W7F, W7F/M131C, and W7F/L135C mutants, which are formed within the burst phase, all have high fluorescence intensity (Figure 6). The I_b intermediates of W7F and W7F/M131C, which are fully formed within 100 ms, are also highly fluorescent, and this fluorescence decays during the slower $I_b \rightarrow N$ transition because of quenching in the native state (Figure 6). In contrast, the fluorescence of the W7F/L135C mutant reaches that of the native state within 100 ms, even though stopped-flow CD shows that refolding to the native state occurs more slowly, at a rate of 2.2 s^{-1}. These results indicate that, similar to the equilibrium molten globule formed at pH 4.5 (Figure 5), the fluorescence of W14 is quenched in the kinetic I_b intermediate, as would be expected if the H helix were shifted toward its N-terminus to bring the side chain of C135 into non-native contact with W14. Thus, fluorescence quenching provides strong evidence of non-native H helix translocation in both the kinetic and equilibrium intermediates of apomyoglobin (apoMb).

Given the evidence of non-native G/H helix packing in the I_b intermediate, we then asked what effect the S108C/L135C disulfide constraint would have on folding kinetics. Stopped-flow traces for refolding of wild-type, reduced, and oxidized (disulfide-bridged) S108C/L135C mutant apomyoglobin were measured by monitoring the change in fluorescence of the two tryptophans following dilution from 8 to 1.3 M urea (Figure 7A). Under these conditions, with a final urea concentration of

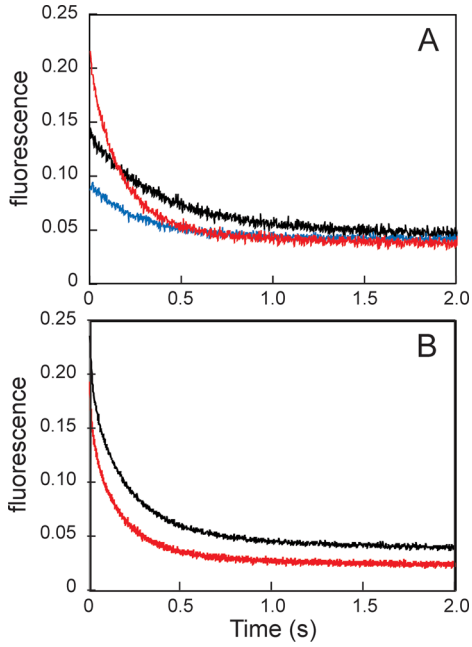

Figure 7. Stopped-flow fluorescence data. (A) Intensity decay curves for wild-type apomyoglobin (black), the oxidized two-cysteine mutant (red), and the reduced two-cysteine mutant (blue) from a urea jump experiment (8 M → 1.3 M). Curves have been scaled to give a similar final value of fluorescence intensity, to allow visual comparison of the relative rates. Estimates of burst phase amplitudes cannot be obtained from these data. (B) Fluorescence decay for wild-type apomyoglobin and the oxidized two-cysteine mutant following a pH jump (from pH 2.5 to 6.0).

1.3 M, I_b is unstable and the kinetics reflect folding of I_a to the native state.[23] Formation of the disulfide increases the overall folding rate nearly 2-fold (Table 2). To examine the effects of the disulfide on the rates of formation and decay of the I_b intermediate, refolding rates were also measured for WT apoMb and the oxidized S108C/L135C mutant by monitoring the change in tryptophan fluorescence following a pH jump from pH 2.5 to 6 (Figure 7B). The data were fit to double-exponential decays, as described above. The rates of both the $I_a \rightarrow I_b$ and $I_b \rightarrow N$ steps were increased 20−30% by the disulfide (Table 2).

Selection of Suitable Fluorescence Acceptor Sites for FRET. Having established that the H helix is translocated toward its N-terminus in both the kinetic and equilibrium intermediates of apoMb, we turned to FRET experiments to obtain an estimate of the magnitude of helix movement. For FRET experiments, the fluorescence acceptor AEDANS was covalently attached at single cysteine residues introduced by mutagenesis at selected sites into the W7F mutant protein. The remaining tryptophan, W14, acts as the fluorescence donor.

A total of 10 fluorescence acceptor sites were evaluated by recording the emission of the incorporated AEDANS at 477 nm (with excitation at 338 nm) as a function of pH. The results (Figure 8) show that the AEDANS-derivatized mutants fall into two groups. All of the mutants exhibit a monotonic increase in fluorescence emission intensity from pH 2 to 4, attributed to a

dx.doi.org/10.1021/bi500478m | Biochemistry 2014, 53, 3767−3780

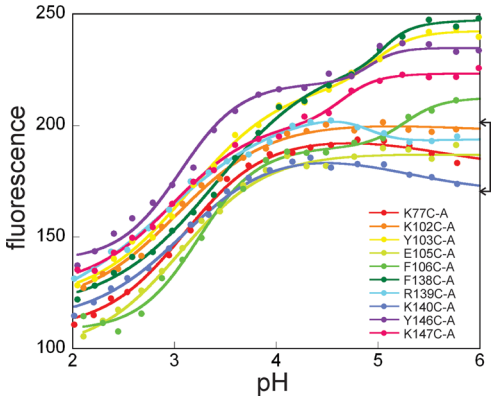

Figure 8. Direct emission from the incorporated IAEDANS as a function of pH for the mutants indicated. A set of mutants that showed no additional AEDANS fluorescence increase between pH 4 and 6 are bracketed. The excitation wavelength was set at 338 nm, and the fluorescence emission was observed at the emission maximum close to 480 nm.

decrease in the extent of solvent exposure of the probe between the acid-unfolded and the molten globule intermediate states. Between pH 4 and 6, one group of mutants (Y103C-A, F106C-A, F138C-A, Y146C-A, and K147C-A, where the A denotes coupling of AEDANS to the introduced Cys residue) shows a further increase in emission intensity, because of further desolvation of the AEDANS probe as the protein folds to the native state. Indeed, with the exception of K147, these residues are all fully or partly buried in the native myoglobin structure.[51] Residues in the second group (K77C-A, K102C-A, E105C-A, R139C-A, and K140C-A) show only a small change in the AEDANS fluorescence intensity between pH 4 and 6, suggesting solvent exposure of the incorporated AEDANS probe as the protein folds from the intermediate to the native state.

Fluorescence and FRET of Apomyoglobin. Fluorescence emission spectra of several of the AEDANS-derivatized W7F mutants were recorded in 6 M urea, in the acid-denatured state at pH 2, and in the molten globule and native states at pH 4 and 6, respectively. Representative spectra for the AEDANS-coupled K77C-A and K140C-A mutants are shown in Figure 9. The fluorescence spectra in 6 M urea (black trace) show two maxima, corresponding to fluorescence emission by W14 (at ~350 nm) and AEDANS (at ~490 nm). Even when the protein is unfolded in 6 M urea, a basal level of resonance energy transfer occurs from W14 to AEDANS. This energy transfer is relatively independent of the location of the AEDANS acceptor and arises through transient sampling of partially collapsed states within the unfolded conformational ensemble. Energy transfer also occurs in the acid-unfolded state at pH 2 (red traces), but its efficiency is strongly dependent upon the location of the AEDANS probe. For K77C-A, there is very little difference between the spectra in 6 M urea and in the absence of urea at pH 2, but at pH 4 (blue trace) and pH 6 (green trace), the emission at ~480 nm is greatly increased and that at ~330 nm decreased, because of efficient energy transfer in the collapsed molten globule and native states. By contrast, the spectrum of K140C-A at pH 2 in the absence of urea is markedly different from that of the urea-denatured form, with a greater emission at ~480 nm due to FRET arising from transiently collapsed states in which there are contacts between the A and H helix regions. These interactions have been described previously on the basis of paramagnetic broadening effects of nitroxide spin-label probes.[52] The 480 nm emission at pH 4 is greater than that at pH 6, showing that the W14 donor and AEDANS acceptor are closer in the molten globule state than in the native state. These observations provide important clues about the structure of the intermediate as well as the presence of long-range contacts involving W14 even in the pH 2 unfolded state.

pH Dependence of FRET. FRET measurements were performed as a function of pH for all of the AEDANS-derivatized W7F apoMb mutants. The W14 fluorescence emission intensity at 336 nm (with excitation at 280 nm) was measured for each cysteine mutant in the absence (intensity = F_0) and presence of the coupled AEDANS acceptor (intensity = F). The FRET efficiency, E, was calculated from the ratio of these values ($E = 1 - F/F_0$). The variation of F/F_0 with pH is shown for the complete set of mutants in Figure S3 of the Supporting Information, and the variation in FRET efficiency E is shown for a subset of mutants in Figure 10A. For all AEDANS derivatives, the FRET efficiency increases (F/F_0 decreases) as the pH is increased from 2 to ~4, accompanying the transition from the acid-unfolded state to the molten globule state. There is a distinct maximum at ~pH 4 in the FRET efficiency versus pH profile for R139C-A and K140C-A (Figure 10), showing clearly that the W14 donor−AEDANS acceptor distance is shorter in the molten globule state than it is in the native state. While probes at some other locations also

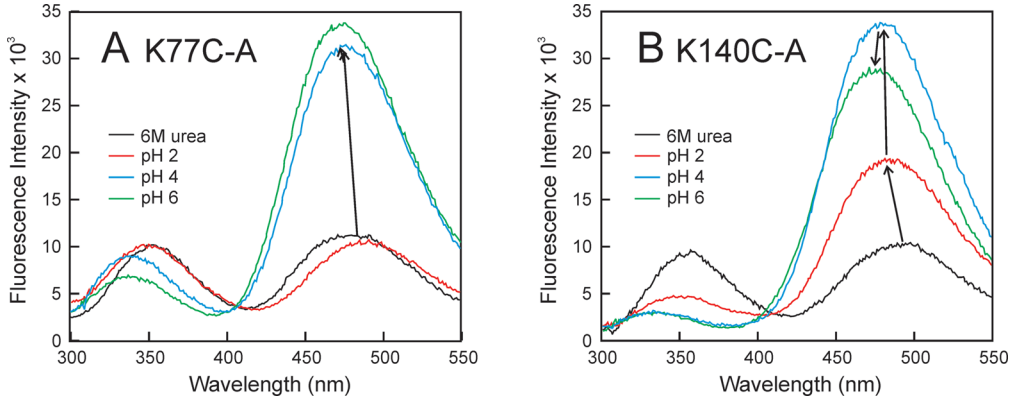

Figure 9. Fluorescence spectra of the AEDANS-substituted mutants under various conditions of pH and presence of denaturant: (A) K77C-A and (B) K140C-A.

dx.doi.org/10.1021/bi500478m | *Biochemistry* 2014, 53, 3767−3780

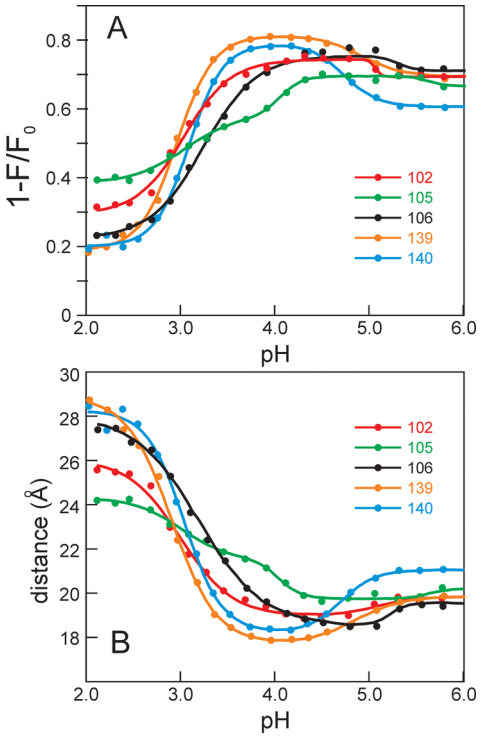

Figure 10. (A) pH dependence of FRET from W14 (A helix) to the AEDANS fluorescence acceptor covalently attached at the mutated cysteine residue for mutants K102C-A (red), E105C-A (green), F106C-A (black), R139C-A (orange), and K140C-A (blue). The FRET efficiency is given by $E = 1 - F/F_0$, where F and F_0 are the W14 emission intensities, measured at the fluorescence maximum close to 338 nm, in the presence and absence of the coupled AEDANS acceptor, respectively. (B) Distances derived from fluorescence energy transfer. The excitation wavelength was 280 nm. Distances were calculated from the FRET efficiencies in panel A using the Förster equation with an R_0 of 22 Å and a κ^2 of 0.67.

exhibit maximal FRET around pH 4−4.5, the maximum is far less pronounced, showing that the structural changes between the molten globule and native states are far smaller than those experienced by probes in the middle of the H helix.

To obtain an estimate of the magnitude of the structural changes, we calculated the donor−acceptor distance in the molten globule and native states using the Förster equation with the R_0 value set at 22 Å for the Trp-AEDANS FRET pair and assuming a dipole orientation factor κ^2 of $^2/_3$.[37] The results are summarized in Table 3. Clearly, the assumption that the AEDANS acceptor is randomly oriented ($\kappa^2 = {}^2/_3$) is unlikely to be appropriate for all locations of the probe, as discussed in detail below. However, the overall result is clear: there is a substantial movement of the central region of the H helix away from the W14 indole ring on progressing from the molten globule to the native state.

This structural change is most obvious from the FRET data for residues located in the central regions of the G and H helices. Chemical shifts and $\{^1H\}-^{15}N$ heteronuclear NOEs show that residues 104−114 (G), 132−143 (H), and 5−15 (A helix region) are nearly fully helical and are packed to form the molten globule core.[9,12,21] During the transition from the molten globule to the native state, energy transfer from W14 to the AEDANS probes coupled at E105C and F106C changes very little (Figure 10). Thus, these probes remain relatively fixed distances from the tryptophan ring, moving only 0.2 and

Table 3. Donor−Acceptor Distances[a] Calculated from FRET Efficiencies

residue	MG (Å)	native (Å)	Δr^b (Å)
K77	19.2	17.6	−1.6
K102	18.4	19.2	0.8
Y103	18.2	19.6	1.4
E105	19.2	19.4	0.2
F106	18.0	18.9	0.9
R139	17.2	19.1	1.9
K140	17.7	20.4	2.7
Y146	18.1	19.4	1.3
K147	19.2	20.2	1.0

[a]Distances were calculated assuming a κ^2 of $^2/_3$ and an R_0 of 22 Å for the Trp-AEDANS pair.[37] [b]Δr is the change in distance between the molten globule and native states.

0.9 Å, respectively (Table 3). In marked contrast, the FRET efficiency decreases substantially for K140C-A and R139C-A, corresponding to movement of the probe away from W14 by 2.7 and 1.9 Å, respectively. The FRET data for these residues thus provide strong evidence of the movement of the H helix relative to the G helix, which itself maintains a fixed position with respect to W14, during the transition from the molten globule to the native state. The side chain of R139 is partially buried in the cleft between the G and H helices, and the assumption that $\kappa^2 = {}^2/_3$ is unlikely to be valid for the AEDANS probe coupled at R139C; the FRET data for R139C-A are therefore only useful as a qualitative indicator of conformational change. In contrast, the AEDANS group coupled at K140C is highly likely to be randomly oriented on the protein surface, and the assumption that $\kappa^2 = {}^2/_3$ is expected to be valid. The X-ray structure shows that the K140 side chain extends away from the protein surface and into the solvent, where it can undergo unimpeded conformational averaging. We therefore used the FRET data for the K140C-A derivative to estimate the magnitude of the helix movement. If we assume that this movement involves sliding of the H helix along its axis, as suggested by previous mutagenesis data[19] and the fluorescence quenching experiments described above, we can estimate an approximate distance through which the H helix must slide to satisfy the FRET constraints. Basic trigonometry indicates that sliding of the H helix toward its N-terminus by one helical turn (5.4 Å) from its position in the native myoglobin structure would shorten the distance between the edge of the W14 ring and the Cα atom of residue 140 by 2.6 Å, in remarkable agreement with the change in distance (2.7 Å) between the native and molten globule states determined from FRET to the K140C-A probe. Obviously, the actual distances measured in the FRET experiments are to the chromophore of the AEDANS acceptor, which is expected to project into the solvent in a direction that is, on average, approximately orthogonal to the helix axis. However, simple geometric considerations indicate that the change in distance reported by the chromophores will be similar to that calculated for the Cα atoms. We thus conclude that the FRET measurements with AEDANS coupled at K140C are consistent with sliding of the central region of the H helix in an N-terminal direction by approximately one helical turn in the molten globule state.

The AEDANS probes at K77C, K102C, Y103C, F146C, and K147C also reflect conformational changes between the molten globule and native states (Figure S3 of the Supporting Information) but likely do not report on H helix translocation.

dx.doi.org/10.1021/bi500478m | Biochemistry 2014, 53, 3767−3780

K102 and Y103 are located in the dynamically frayed N-terminal region of helix G,[18] which is only ~50% helical in the molten globule, averages over both helical and more extended states in the conformational ensemble, and exhibits enhanced amide proton exchange.[9,12,21] Similarly, in the molten globule state, residues Y146 and K147 are located C-terminal to the well-folded helical core of helix H, in a region that is strongly frayed and highly dynamic. The distance changes reported by FRET probes at K102C, Y103C, F146C, and K147C are thus more likely to reflect stabilization of structure at the ends of the G and H helices upon folding to the native state, rather than H helix translocation. Finally, the AEDANS probe at K77C is located near the C-terminal end of helix E, in a region that is partially compacted but highly disordered in the molten globule.[9,12] The distance between K77C-A and W14 decreases further at pH 6, showing that the structure in this region becomes more compact in the native state.

DISCUSSION

Folding Pathway of Apomyoglobin. The kinetic folding pathway of apomyoglobin has been studied extensively by stopped-flow and quench-flow methods.[7,11,14,18−20,22−25,53−55] Following the pH jump to pH 6, acid-unfolded apomyoglobin refolds via two sequential kinetic intermediates that, following Jamin and Baldwin, we herein designate I_a and I_b.[22−25] Intermediate I_a accumulates within the burst phase of a conventional stopped-flow instrument, as used in this work, but its formation can be observed directly using submillisecond continuous-flow mixing devices.[22,24,25,55] Recent studies have revealed an additional intermediate, formed 30−40 μs after initiation of refolding, between the unfolded state and I_a.[55] Because this intermediate is too transient to be observed in our experiments, we analyze our data using a simplified folding pathway: U ↔ I_a ↔ I_b ↔ N.

Ultrafast hydrogen−deuterium exchange pulse labeling experiments revealed an ensemble of intermediate states that interconvert in a hierarchical manner as apomyoglobin folds.[22] A compact intermediate formed within 400 μs of refolding, corresponding to I_a, contains helical structure in the A, G, and H regions. After 6 ms, additional structure is stabilized in parts of the B, C, and E helix regions as intermediate I_b becomes populated. This latter intermediate is a heterogeneous, kinetically trapped state in which folding is impeded by energetic frustration in the B−G and G−H helix interfaces, which affects docking and stabilization of the E helix.[19,20] On the basis of mutagenesis of core hydrophobic residues, it has been suggested that the H helix is translocated, relative to G, by approximately one helical turn toward its N-terminus to maximize burial of hydrophobic residues.[19] I_b is also formed transiently during unfolding and refolding under equilibrium conditions at pH 4.8−5.0.[21]

The molten globule state that is populated at equilibrium under mildly acidic conditions (pH ~4) shares structural similarity with intermediates formed during kinetic refolding.[7−9,14,56] Direct NMR and hydrogen exchange experiments show that the equilibrium molten globule contains a large population of helical structure in the A, B, G, and H helix regions, with the remainder of the polypeptide chain being highly dynamic.[9,12,18,21] The pH 4 intermediate is structurally heterogeneous and consists of an equilibrium mixture of intermediates I_a and I_b that are observed in kinetic experiments;[23,55] pressure causes a shift in the equilibrium to favor the I_a state.[57]

Although the translocation of the H helix in the intermediate folded state was inferred from previous data, there was no prima facie evidence of it. The fluorescence quenching experiments reported in this work provide direct evidence of this process, which leads to non-native contacts between the A and H helix regions in both the equilibrium molten globule and I_b kinetic intermediate. Incorporation of a cysteine quencher in adjacent turns of the H helix reveals close, non-native contacts between residue 135 and W14 in the equilibrium molten globule that are relaxed in the native state (Figure 5). In the stopped-flow fluorescence experiments shown in Figures 6 and 7, an increase in fluorescence intensity occurs within the dead time (~5 ms), due to formation of intermediate I_a. The fluorescence then decreases during a fast kinetic phase as I_a progresses to I_b, with a further decrease as I_b folds to the native state (N) during the slow refolding phase. For the W7F/L135C mutant, the W14 fluorescence is strongly quenched in the I_b intermediate, showing that the non-native interactions observed in the equilibrium molten globule are also present in the kinetic I_b intermediate. In contrast, the I_a intermediate of W7F/L135C exhibits fluorescence comparable to that of the W7F or W7F/M131C mutant, indicating that the close contacts between residue 135 and W14 have not yet formed in I_a. This may reflect fluctuations within the A−G−H core of I_a that decrease the probability of C135−W14 contacts, or packing of the helices in a non-native topology. Enhanced opening rates to amide exchange-competent states are observed for the central residues of the H helix in the I_a intermediate, confirming the presence of conformational fluctuations.[22]

The fluorescence quenching experiments provide unequivocal evidence of translocation of the H helix toward its N-terminus in both the pH 4.1 molten globule and the kinetic I_b intermediate but do not provide a direct measure of the magnitude of the helix movement. To address this question, we turned to FRET experiments with W7F apomyoglobin, using probes located in regions of the G and H helices that are highly helical and packed against the compact hydrophobic core of the equilibrium molten globule. The efficiency of energy transfer from W14 to AEDANS probes coupled at R139C and K140C, within the H helix, is maximal over the pH range at which the equilibrium molten globule is populated and decreases upon folding to the native state (Figure 10A). In contrast, probes in the central, folded region of the G helix do not change position relative to W14 over this pH range, suggesting that the packing between the core regions of the A and G helices remains relatively fixed in the molten globule and native states. Quantitative analysis of the FRET data for AEDANS coupled at the fully solvent exposed K140C, for which the assumption of random AEDANS orientation is expected to be valid, shows that the probe is 2.7 Å closer to W14 in the molten globule than in native apomyoglobin (Table 3 and Figure 10B). Assuming a model in which the H helix slides along its axis, as illustrated in Figure 11, this decrease in distance is consistent with movement of the H helix by approximately one helical turn (5.4 Å) toward its N-terminus. A movement of this magnitude would bring the L135C side chain close to the indole ring of W14, consistent with the enhanced fluorescence quenching observed for the equilibrium molten globule and I_b intermediate of the W7F/L135C mutant.

Effect of the G−H Disulfide Bridge on Backbone Structure and Dynamics. To explore the role of H helix translocation in the folding pathway of apomyoglobin, we designed and characterized a double-cysteine mutant for which

dx.doi.org/10.1021/bi500478m | Biochemistry 2014, 53, 3767−3780

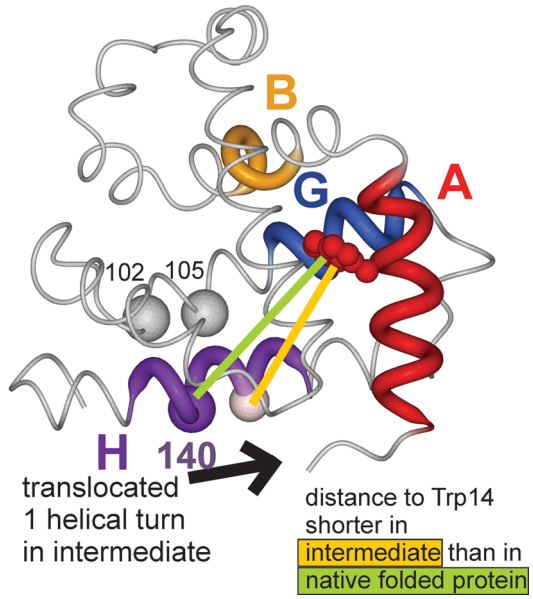

Figure 11. Schematic diagram illustrating how a translocation of the H helix toward the N-terminus by approximately one helical turn decreases the distance between a fluorescence acceptor at position 140 and the donor W14 in the molten globule intermediate compared to the folded state. The backbone structure of myoglobin[51] is colored to show the regions of the protein that are folded and protect amides from exchange in the burst phase intermediate.[18,22,61] Helix colors correspond to those in Figure 1. The distances between the Cα atom of residue 140 in the "native" and "translocated" forms of the H helix are shown schematically as green and yellow lines, respectively. The position of K140 in the translocated H helix is modeled by the Cα atom of L137 for illustrative purposes.

the oxidized disulfide form would lock the register of the G and H helices into the "nativelike" state present in the fully folded protein.

The overall folded structure and backbone flexibility of the oxidized S108C−L135C mutant are similar to those of the wild-type protein at pH 6.1, and the residual helical structure and overall level of folded structure remain similar at pH 4.1 (Figures 2 and 4 and Figures S1 and S2 of the Supporting Information). The ^{1}H and ^{15}N chemical shifts for the wild-type and disulfide-bridged proteins are very similar, and differences in shifts are small and mainly localized to the G and H helices surrounding the mutation sites (Figure 2). Perturbed chemical shifts are observed at pH 4.1 at sites in the N- and C-terminal ends of both the G and H helices (Figure 2B). The juxtaposition of these sites in the H helix onto those that show shift perturbations in helix G provides evidence that the H helix is in a nativelike position in the equilibrium intermediate of the oxidized disulfide mutant protein. We conclude that the disulfide bond fixes the register of the G and H helices relative to each other into the position that they take up in the fully folded apoprotein.

Local deviation of ^{13}Cα chemical shifts from random coil values (termed secondary shift) gives information about the secondary structure propensity of the backbone. Downfield shifts, which yield positive values for the quantity $\delta_{obs} - \delta_{rc}$, are characteristic of helical structure.[58,59] The secondary ^{13}Cα chemical shifts at pH 6.1 are very similar to those of the WT, indicating a high degree of similarity in helical content between the disulfide mutant and the wild-type protein; this agrees well with the CD data at pH 6.1 (Figure 4A). The ^{13}Cα secondary chemical shifts for the disulfide mutant at pH 4.1 (Figure 3A) have a pattern similar to that of the chemical shifts of the WT with some exceptions localized to the G and H helices. Under these conditions, where formation of the equilibrium folding intermediate is maximal,[7] ^{13}Cα shift changes (Figure 3B) indicate an increase in helicity at the N-terminus of the H helix (residues 125−129) and at the C-terminus of the G helix, in residues that contact the N-terminus of helix H in the native fold. In contrast, the C-terminal region of the H helix shows somewhat lower helicity in the disulfide-bridged mutant protein at pH 4.1.

Changes in backbone dynamics as a consequence of the formation of the disulfide bond were investigated by measuring {^{1}H}−^{15}N heteronuclear NOEs, which provide information about the amplitudes of local picosecond to nanosecond motions of the amide bond. Large positive NOEs indicate areas of the protein with restricted motions on this time scale, while lower values indicate more flexible regions of the backbone. Restriction of local motion can be caused by polypeptide chain collapse and packing interactions within the compact core of the molten globule.[9] The pattern of heteronuclear NOEs for the disulfide-bonded mutant protein is similar to that of the WT at pH 4.1, but for many residues, the values observed for the mutant are higher than for the WT (Figure 3C). Significantly increased NOEs are found in the C-terminal half of the G helix, the G−H turn, and the N-terminal half of the H helix, corresponding to a restriction of motion resulting from the stabilization of helical structure in this region through formation of the disulfide bond. A small but significant increase in the NOE values is also observed for several residues in the N-terminus and in helix A, in a region that contacts the N-terminus of helix H and the G−H turn in the native myoglobin fold.

Interestingly, the largest increase in the extent of motional restriction is observed for several E helix residues (Figure 3C). The heteronuclear NOEs observed for E helix residues in the WT equilibrium intermediate are negative or only weakly positive, suggesting that the E helix is highly dynamic and makes only transient interactions with the compact molten globule core[9,12] (Figure 3C, black line). By contrast, there is a marked increase in the heteronuclear NOEs for several residues in the E helix region of the disulfide mutant (Figure 3C, red line), to values that approach the magnitude of the NOEs observed for many residues in the A, G, and H helices. In particular, large increases in the NOE are observed for L72, I75, and L76. In the native myoglobin fold, these side chains anchor the C-terminus of helix E to helix H through hydrophobic contacts with the side chains of M131, L135, and F138. Translocation of the H helix by one turn toward its N-terminus in the wild-type molten globule would cause a steric clash between F138 and the E helix side chains, destabilizing E−H helix packing and frustrating the folding process. By constraining the H helix in its native position, the S108C/L135C disulfide bond promotes nativelike docking of the C-terminal hydrophobic residues of helix E. Residues T67 and V68 in the middle of the E helix also exhibit more restricted motions in the disulfide-bridged molten globule, as does a cluster of residues in helix F that contact the C-terminal ends of the E and H helices in the native fold.

Although the nativelike G−H helix topology facilitates packing of the E helix onto the hydrophobic core, the secondary ^{13}Cα chemical shifts do not increase significantly, indicating that helical structure in E is not increased. The E

dx.doi.org/10.1021/bi500478m | *Biochemistry* 2014, 53, 3767−3780

helix region remains highly dynamic in the mutant, and docking to the ABGH core appears to be driven largely by hydrophobic contacts. Quench-flow experiments on hydrophobic core mutants of apomyoglobin revealed considerable heterogeneity in packing of the E helix against the ABGH core in the burst phase intermediate, with L69 and L72 making both native and non-native contacts.[19] Heterogeneity in the B−E, E−G, and E−H helix contacts in the acid molten globule has recently been confirmed by direct measurement of distances between spin-label probes.[60]

The formation of a disulfide bond between the side chains at positions 108 and 135 facilitates interactions between the G and H helix regions even in the acid-unfolded states of the mutant protein, causing an increase in the level of residual helical structure observed at pH 2 (Figure 4A). There is a slight destabilization of the native folded state when the pH is decreased from 6.1 to 4.1 (Figure 4A), resulting in an increased pH range over which the equilibrium (pH 4.1) intermediate is present. Nevertheless, the amount of residual helical structure at pH 4.1 is identical for mutant and wild-type proteins, as indicated by the similarity of the ellipticity at this pH. By contrast, the fluorescence intensity of the two proteins differs markedly at pH 4.1 and 6.1 (Figure 4B), reflecting differences in the quenching of the fluorescence of W7 and W14 by the presence of the disulfide bond in both the molten globule and native states.

Effect of the 108−135 Disulfide on Apomyoglobin Folding Kinetics. The NMR and CD data indicate clearly that the S108C−L135C disulfide facilitates interactions between the G and H helix regions in the acid-unfolded state and prevents H helix translocation in the pH 4 molten globule, resulting in nativelike G−H helix packing. Naively, one might expect that the relief of energetic frustration in the G−H interface of the disulfide-bonded molten globule would lead to faster folding. Indeed, folding of the disulfide-bridged apomyoglobin is faster, but only slightly (Table 2). The overall refolding rate following urea dilution is increased 2.5-fold over that of the wild-type protein, and the rates of the individual $I_a \rightarrow I_b$ and $I_b \rightarrow N$ steps, observed in pH jump experiments, are each increased 20−30% by the disulfide. This modest increase in rate upon relief of the non-native G−H helix packing points to additional sources of energetic frustration that slow the folding process. Previous work has shown that correct packing and folding of the E helix is required before the folding transition state can be reached.[19] While constraining the H helix in a native position in the molten globule by the S108C−L135C disulfide facilitates E helix docking, it does not by itself promote E helix folding (there is no increase in helicity), and the E helix residues remain dynamically disordered. Clearly, additional sites of energetic frustration must be relieved before the E helix can properly dock and fold to allow progression to the transition state.

Previous mutagenesis experiments provide insights into additional interactions that frustrate apomyoglobin folding. The intermediates observed during kinetic refolding of apomyoglobin constitute heterogeneous ensembles of compact, kinetically trapped states in which the helix packing appears to be topologically correct but in which there are local non-native interactions that must be resolved before the protein can fold to the native structure.[16,19,22] Three sites of energetic frustration have thus far been identified that impede native docking interactions of helix E and progression to the transition state: non-native G−H helix packing,[19] instability at the N-terminus of helix B,[20] and burial of the distal His64.[13] Relief of all three sources of frustration is required before folding can be completed; mutations that resolve the frustration at only one of the sites result in at best an only ∼2-fold increase in the folding rate. Conversely, mutations in the F helix region that stabilize the misfolded AGH intermediate and inhibit translocation of the H helix to its native position decrease the overall folding rate by up to 6-fold.[53]

Stable docking of the E helix is a pivotal step in the apomyoglobin folding pathway, and mutations that impede this process slow the overall folding rate.[19] Ultrafast quench-flow H−D exchange measurements show that amides at the N- and C-terminal regions of the E helix become protected at different rates during refolding.[22] The C-terminal residues, which contact helix H in the native structure, fold more rapidly than the N-terminal part of helix E, which appears to fold concomitantly with the N-terminus of the B helix with which it is in direct contact in the native folded state. Mutations that stabilize the N-terminus of helix B, namely, G23A/G25A and H24L/H119F, promote nativelike interactions with the C-terminus of helix G and the N-terminal region of E, leading to propagation and stabilization of helical structure throughout helix E.[20] Thus, docking and folding of helix E is a cooperative process, in which nativelike interactions must be formed in both the B−E−G and E−G−H interfaces before stable helical structure can form. This is seen clearly in our current data, where resolution of non-native structure in the G−H interface leads only to enhancement of hydrophobic contacts with residues in the C-terminus of helix E, with no stabilization of helical structure. We conclude that progression to the rate-determining step for apomyoglobin folding cannot be associated exclusively either with overcoming non-native H helix interactions or with correct docking of the E helix onto the folded B−G helix interface. Instead, the folding transition state is likely reached via multiple pathways, providing further evidence that the apomyoglobin folding landscape is highly rugged and involves much energetic frustration.

The results of this study are consistent with a mechanism in which the collapsing polypeptide chain maximizes burial of hydrophobic residues in the A−G−H helix interface, resulting in a compact state in which the H helix is translocated relative to the G and A helices. This constitutes a kinetic trap, which is likely resolved by localized unfolding that allows the helix to slide to its native position, rather than through a global unfolding process. Such a model is consistent with the increased H helix opening rates, relative to the core regions of the A and G helices, revealed by quenched-flow hydrogen−deuterium exchange.[22]

The translocation of the helix in the equilibrium molten globule and the kinetic I_b intermediate appears to promote disorder in the E and F helices. Movement of the H helix into its native docking site on helix G relieves the energetic frustration in the E−H helix interface and promotes docking of hydrophobic residues at the C-terminal end of helix E and in helix F. However, as discussed above, this in itself is insufficient for proper docking and stabilization of helical structure in helix E.

The results reported here, in conjunction with a wealth of published data, greatly advance our understanding of apomyoglobin folding pathways and the consequences of energetic frustration. The folding landscape is highly rugged, with several energetic bottlenecks that frustrate the folding process. Relief of any one of the major identified bottlenecks, in

the E−G−H and B−E−G helix interfaces, is insufficient to speed progression to the transition state. It is also notable that when frustration is relieved at either of these sites by introduction of a disulfide, as in the work presented here, or by mutagenesis in the B−G helix interface,[20] it does not lead to excessive stabilization of the frustrated E helix. Rather, the resulting stabilization of E helix contacts is incremental, and the polypeptide chain in this region remains dynamically disordered, allowing it to search conformational space efficiently until additional sources of frustration are relieved and E helix folding can be completed. This progressive decrease in chain flexibility, accompanied by the progressive accumulation of secondary structure, likely facilitates folding by preventing excessive stabilization of non-native contacts within the ensemble of compact folding intermediates.

■ ASSOCIATED CONTENT

Supporting Information

A table showing expression behavior of double-cysteine mutants and supplementary figures. This material is available free of charge via the Internet at http://pubs.acs.org.

■ AUTHOR INFORMATION

Corresponding Author

*Department of Integrative Structural and Computational Biology and Skaggs Institute for Chemical Biology, The Scripps Research Institute, 10550 N. Torrey Pines Rd., La Jolla, CA 92037. E-mail: wright@scripps.edu. Telephone: (858) 784-9721. Fax: (858) 784-9822.

Author Contributions

P.C.A. and C.N. contributed equally to this work.

Funding

This work was supported by National Institutes of Health Grant DK34909.

Notes

The authors declare no competing financial interest.

■ ACKNOWLEDGMENTS

We thank Gerard Kroon for his assistance with NMR experiments and Maria Martinez-Yamout and Euvel Manlapaz for helpful discussion and assistance in sample preparation.

■ ABBREVIATIONS

Mb, myoglobin; apoMb, apomyoglobin; FRET, Förster resonance energy transfer; CD, circular dichroism; AEDANS, 5-({2-[(acetyl)amino]ethyl}amino)naphthalene-1-sulfonic acid; NOE, nuclear Overhauser enhancement.

■ REFERENCES

(1) Udgaonkar, J. B., and Baldwin, R. L. (1988) NMR evidence for an early framework intermediate on the folding pathway of ribonuclease A. *Nature 335*, 694−699.

(2) Roder, H., Elöve, G. A., and Englander, S. W. (1988) Structural characterization of folding intermediates in cytochrome *c* by H-exchange labelling and proton NMR. *Nature 335*, 700−704.

(3) Lyon, C. E., Suh, E. S., Dobson, C. M., and Hore, P. J. (2002) Probing the exposure of tyrosine and tryptophan residues in partially folded proteins and folding intermediates by CIDNP pulse-labeling. *J. Am. Chem. Soc. 124*, 13018−13024.

(4) Balbach, J., Forge, V., van Nuland, N. A. J., Winder, S. L., Hore, P. J., and Dobson, C. M. (1995) Following protein folding in real time using NMR spectroscopy. *Nat. Struct. Biol. 2*, 865−870.

(5) Balbach, J. (2000) Compaction during protein folding studied by real-time NMR diffusion experiments. *J. Am. Chem. Soc. 122*, 5887−5888.

(6) Mizuguchi, M., Kroon, G. J., Wright, P. E., and Dyson, H. J. (2003) Folding of a β-sheet protein monitored by real-time NMR spectroscopy. *J. Mol. Biol. 328*, 1161−1171.

(7) Jennings, P. A., and Wright, P. E. (1993) Formation of a molten globule intermediate early in the kinetic folding pathway of apomyoglobin. *Science 262*, 892−896.

(8) Eliezer, D., Jennings, P. A., Wright, P. E., Doniach, S., Hodgson, K. O., and Tsuruta, H. (1995) The radius of gyration of an apomyoglobin folding intermediate. *Science 270*, 487−488.

(9) Eliezer, D., Yao, J., Dyson, H. J., and Wright, P. E. (1998) Structural and dynamic characterization of partially folded states of apomyoglobin and implications for protein folding. *Nat. Struct. Biol. 5*, 148−155.

(10) Cavagnero, S., Dyson, H. J., and Wright, P. E. (1999) Effect of H helix destabilizing mutations on the kinetic and equilibrium folding of apomyoglobin. *J. Mol. Biol. 285*, 269−282.

(11) Tsui, V., Garcia, C., Cavagnero, S., Siuzdak, G., Dyson, H. J., and Wright, P. E. (1999) Quench-flow experiments combined with mass spectrometry show apomyoglobin folds through an obligatory intermediate. *Protein Sci. 8*, 45−49.

(12) Eliezer, D., Chung, J., Dyson, H. J., and Wright, P. E. (2000) Native and non-native secondary structure and dynamics in the pH 4 intermediate of apomyoglobin. *Biochemistry 39*, 2894−2901.

(13) Garcia, C., Nishimura, C., Cavagnero, S., Dyson, H. J., and Wright, P. E. (2000) Changes in the apomyoglobin folding pathway caused by mutation of the distal histidine residue. *Biochemistry 39*, 11227−11237.

(14) Nishimura, C., Dyson, H. J., and Wright, P. E. (2002) The apomyoglobin folding pathway revisited: Structural heterogeneity in the kinetic burst phase intermediate. *J. Mol. Biol. 322*, 483−489.

(15) Kitahara, R., Yamada, H., Akasaka, K., and Wright, P. E. (2002) High pressure NMR reveals that apomyoglobin is an equilibrium mixture from the native to the unfolded. *J. Mol. Biol. 320*, 311−319.

(16) Nishimura, C., Wright, P. E., and Dyson, H. J. (2003) Role of the B helix in early folding events in apomyoglobin: Evidence from site-directed mutagenesis for native-like long range interactions. *J. Mol. Biol. 334*, 293−307.

(17) Cavagnero, S., Nishimura, C., Schwarzinger, S., Dyson, H. J., and Wright, P. E. (2001) Conformational and dynamic characterization of the molten globule state of an apomyoglobin mutant with an altered folding pathway. *Biochemistry 40*, 14459−14467.

(18) Nishimura, C., Dyson, H. J., and Wright, P. E. (2005) Enhanced picture of protein-folding intermediates using organic solvents in H/D exchange and quench-flow experiments. *Proc. Natl. Acad. Sci. U.S.A. 102*, 4765−4770.

(19) Nishimura, C., Dyson, H. J., and Wright, P. E. (2006) Identification of native and non-native structure in kinetic folding intermediates of apomyoglobin. *J. Mol. Biol. 355*, 139−156.

(20) Nishimura, C., Dyson, H. J., and Wright, P. E. (2010) Energetic frustration of apomyoglobin folding: Role of the B helix. *J. Mol. Biol. 396*, 1319−1328.

(21) Meinhold, D. W., and Wright, P. E. (2011) Measurement of protein unfolding/refolding kinetics and structural characterization of hidden intermediates by NMR relaxation dispersion. *Proc. Natl. Acad. Sci. U.S.A. 108*, 9078−9083.

(22) Uzawa, T., Nishimura, C., Akiyama, S., Ishimori, K., Takahashi, S., Dyson, H. J., and Wright, P. E. (2008) Hierarchical folding mechanism of apomyoglobin revealed by ultra-fast H/D exchange coupled with 2D NMR. *Proc. Natl. Acad. Sci. U.S.A. 105*, 13859−13864.

(23) Jamin, M., and Baldwin, R. L. (1998) Two forms of the pH 4 folding intermediate of apomyoglobin. *J. Mol. Biol. 276*, 491−504.

(24) Weisbuch, S., Gerard, F., Pasdeloup, M., Cappadoro, J., Dupont, Y., and Jamin, M. (2005) Cooperative sub-millisecond folding kinetics of apomyoglobin pH 4 intermediate. *Biochemistry 44*, 7013−7023.

(25) Uzawa, T., Akiyama, S., Kimura, T., Takahashi, S., Ishimori, K., Morishima, I., and Fujisawa, T. (2004) Collapse and search dynamics of apomyoglobin folding revealed by submillisecond observations of α-helical content and compactness. *Proc. Natl. Acad. Sci. U.S.A. 101*, 1171−1176.
(26) Jennings, P. A., Stone, M. J., and Wright, P. E. (1995) Overexpression of myoglobin and assignment of the amide, Cα and Cβ resonances. *J. Biomol. NMR 6*, 271−276.
(27) Pace, C. N., Vajdos, F., Fee, L., Grimsley, G., and Gray, T. (1995) How to measure and predict the molar absorption coefficient of a protein. *Protein Sci. 4*, 2411−2423.
(28) Nishimura, C., Riley, R., Eastman, P., and Fink, A. L. (2000) Fluorescence energy transfer indicates similar transient and equilibrium intermediates in staphylococcal nuclease folding. *J. Mol. Biol. 299*, 1133−1146.
(29) Marion, D., Ikura, M., Tschudin, R., and Bax, A. (1989) Rapid recording of 2D NMR spectra without phase cycling. Application to the study of hydrogen exchange in proteins. *J. Magn. Reson. 85*, 393−399.
(30) Grzesiek, S., and Bax, A. (1992) Improved 3D triple-resonance NMR techniques applied to a 31 kDa protein. *J. Magn. Reson. 96*, 432−440.
(31) Zhang, O., Kay, L. E., Olivier, J. P., and Forman-Kay, J. D. (1994) Backbone ^{1}H and ^{15}N resonance assignments of the N-terminal SH3 domain of drk in folded and unfolded states using enhanced-sensitivity pulsed field gradient NMR techniques. *J. Biomol. NMR 4*, 845−858.
(32) Farrow, N. A., Muhandiram, R., Singer, A. U., Pascal, S. M., Kay, C. M., Gish, G., Shoelson, S. E., Pawson, T., Forman-Kay, J. D., and Kay, L. E. (1994) Backbone dynamics of a free and a phosphopeptide-complexed Src homology 2 domain studied by ^{15}N NMR relaxation. *Biochemistry 33*, 5984−6003.
(33) Delaglio, F., Grzesiek, S., Vuister, G. W., Guang, Z., Pfeifer, J., and Bax, A. (1995) NMRPipe: A multidimensional spectral processing system based on UNIX pipes. *J. Biomol. NMR 6*, 277−293.
(34) Johnson, B. A., and Blevins, R. A. (1994) NMRView: A computer program for the visualization and analysis of NMR data. *J. Biomol. NMR 4*, 603−614.
(35) Schwarzinger, S., Kroon, G. J. A., Foss, T. R., Chung, J., Wright, P. E., and Dyson, H. J. (2001) Sequence dependent correction of random coil NMR chemical shifts. *J. Am. Chem. Soc. 123*, 2970−2978.
(36) Förster, T. (1946) Zwischenmolekulare energiewanderung und fluoreszenz. *Ann. Phys. 2*, 55−75.
(37) Wu, P., and Brand, L. (1994) Resonance energy transfer: Methods and applications. *Anal. Biochem. 218*, 1−13.
(38) Eliezer, D., and Wright, P. E. (1996) Is apomyoglobin a molten globule? Structural characterization by NMR. *J. Mol. Biol. 263*, 531−538.
(39) Lecomte, J. T., Sukits, S. F., Bhattacharjya, S., and Falzone, C. J. (1999) Conformational properties of native sperm whale apomyoglobin in solution. *Protein Sci. 8*, 1484−1491.
(40) Richardson, J. S. (1981) The anatomy and taxonomy of protein structure. *Adv. Protein Chem. 34*, 167−339.
(41) Thornton, J. M. (1981) Disulphide bridges in globular proteins. *J. Mol. Biol. 151*, 261−287.
(42) Shen, Y., Delaglio, F., Cornilescu, G., and Bax, A. (2009) TALOS+: A hybrid method for predicting protein backbone torsion angles from NMR chemical shifts. *J. Biomol. NMR 44*, 213−223.
(43) Griko, Y. V., Privalov, P. L., Venyaminov, S. Y., and Kutyshenko, V. P. (1988) Thermodynamic study of the apomyoglobin structure. *J. Mol. Biol. 202*, 127−138.
(44) Nishii, I., Kataoka, M., Tokunaga, F., and Goto, Y. (1994) Cold denaturation of the molten globule states of apomyoglobin and a profile for protein folding. *Biochemistry 33*, 4903−4909.
(45) Irace, G., Balestrieri, C., Parlato, G., Servillo, L., and Colonna, G. (1981) Tryptophanyl fluorescence heterogeneity of apomyoglobins. Correlation with the presence of two distinct structural domains. *Biochemistry 20*, 792−799.
(46) Gonnelli, M., and Strambini, G. B. (1995) Phosphorescence lifetime of tryptophan in proteins. *Biochemistry 34*, 13847−13857.
(47) Lapidus, L. J., Eaton, W. A., and Hofrichter, J. (2000) Measuring the rate of intramolecular contact formation in polypeptides. *Proc. Natl. Acad. Sci. U.S.A. 97*, 7220−7225.
(48) Bashford, D., Chothia, C., and Lesk, A. M. (1987) Determinants of a protein fold. Unique features of the globin amino acid sequence. *J. Mol. Biol. 196*, 199−216.
(49) Kay, M. S., and Baldwin, R. L. (1996) Packing interactions in the apomyoglobin folding intermediate. *Nat. Struct. Biol. 3*, 439−445.
(50) Sirangelo, I., Bismuto, E., Tavassi, S., and Irace, G. (1998) Near-ultraviolet circular dichroic activity of apomyoglobin: Resolution of the individual tryptophanyl contributions by site-directed mutagenesis. *Eur. Biophys. J. Biophys. Lett. 27*, 27−31.
(51) Kuriyan, J., Wilz, S., Karplus, M., and Petsko, G. A. (1986) X-ray structure and refinement of carbon-monoxy (Fe II)-myoglobin at 1.5 Å resolution. *J. Mol. Biol. 192*, 133−154.
(52) Felitsky, D. J., Lietzow, M. A., Dyson, H. J., and Wright, P. E. (2008) Modeling transient collapsed states of an unfolded protein to provide insights into early folding events. *Proc. Natl. Acad. Sci. U.S.A. 105*, 6278−6283.
(53) Nishimura, C., Dyson, H. J., and Wright, P. E. (2011) Consequences of stabilizing the natively disordered F helix for the folding pathway of apomyoglobin. *J. Mol. Biol. 411*, 248−263.
(54) Jamin, M., and Baldwin, R. L. (1996) Refolding and unfolding kinetics of the equilibrium folding intermediate of apomyoglobin. *Nat. Struct. Biol. 3*, 613−618.
(55) Xu, M., Beresneva, O., Rosario, R., and Roder, H. (2012) Microsecond folding dynamics of apomyoglobin at acidic pH. *J. Phys. Chem. B 116*, 7014−7025.
(56) Hughson, F. M., Wright, P. E., and Baldwin, R. L. (1990) Structural characterization of a partly folded apomyoglobin intermediate. *Science 249*, 1544−1548.
(57) Lerch, M. T., Horwitz, J., McCoy, J., and Hubbell, W. L. (2013) Circular dichroism and site-directed spin labeling reveal structural and dynamical features of high-pressure states of myoglobin. *Proc. Natl. Acad. Sci. U.S.A. 110*, E4714−E4722.
(58) Wishart, D. S., and Sykes, B. D. (1994) The ^{13}C chemical-shift index: A simple method for the identification of protein secondary structure using ^{13}C chemical-shift data. *J. Biomol. NMR 4*, 171−180.
(59) Spera, S., and Bax, A. (1991) Empirical correlation between protein backbone conformation and Cα and Cβ ^{13}C nuclear magnetic resonance chemical shifts. *J. Am. Chem. Soc. 113*, 5490−5492.
(60) Lerch, M. T., Yang, Z., Brooks, E. K., and Hubbell, W. L. (2014) Mapping protein conformational heterogeneity under pressure with site-directed spin labeling and double electron−electron resonance. *Proc. Natl. Acad. Sci. U.S.A. 111*, E1201−E1210.
(61) Nishimura, C., Lietzow, M. A., Dyson, H. J., and Wright, P. E. (2005) Sequence determinants of a protein folding pathway. *J. Mol. Biol. 351*, 383−392.